

Supporting Information

The dominance of sulfate over two organic ligands in the solvothermal assembly of an undecanuclear cobaltous cluster: crystallography and mass-spectrometry

Li-Ping Jiang,^{a,c} Mohamedally Kurmoo,^{d,} and Ming-Hua Zeng,^{a,b,*}*

^a Key Laboratory for the Chemistry and Molecular Engineering of Medicinal Resources, Department of Chemistry and Pharmaceutical Sciences, Guangxi Normal University, Guilin, 541004, P. R. China

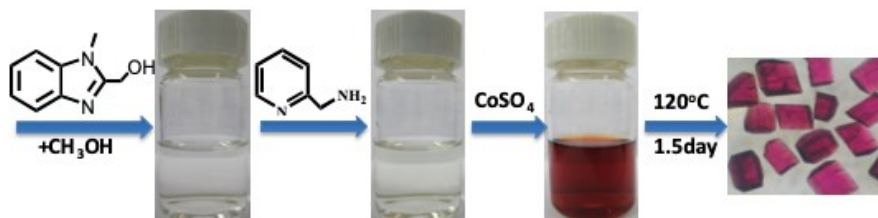
^b Hubei Collaborative Innovation Center for Advanced Organic Chemical Materials, Ministry of Education Key Laboratory for the Synthesis and Application of Organic Functional Molecules, College of Chemistry and Chemical Engineering, Hubei University, Wuhan, 430062, P. R. China

^c College of Chemistry and Bioengineering, Guilin University of Technology, Guilin 541004, P. R. China

^d Université de Strasbourg, Institut de Chimie, CNRS-UMR7177, 4 rue Blaise Pascal, Strasbourg 67008, France

E-mail: kurmoo@unistra.fr; zmh@mailbox.gxnu.edu.cn

Supporting Tables	
Table S1	Statistics of the high nuclear odd cobalt cluster (≥ 10) from the CSD database.
Table S2	Crystallographic data for 1 .
Table S3	Selected bond lengths (Å) and angles (°) of 1 .
Table S4	Major species assigned in the ESI-MS of 1 in negative mode.
Table S5	Time-dependent ESI-MS spectra assigned in the ESI-MS of 1 in negative mode.
Supporting Figures	
Scheme S1	The schematic of the synthetic procedure of 1 .
Figure S1	Statistical graph of the reported coordination models of sulphate with transition metal ions.
Figure S2	View of the coordination geometry of different cobalt ions in 1
Figure S3	View of the coordination model of the <i>mbm</i> and <i>pma</i> ligands.
Figure S4	View of linkage of the [Co ₉] inner core through <i>mbm</i> ⁻ and SO ₄ ²⁻ .
Figure S5	View of the packing model of 1 along different crystallographic axis.
Figure S6	The measured and simulated PXRD data for 1 .
Figure S7	Infrared transmission spectrum of 1 .
Figure S8	Thermogravimetry of 1 at a heating rate of 5 °C/min under N ₂ atmosphere.
Figure S9	Negative ESI-MS spectra of 1 in CH ₃ OH.
Figure S10	The superposed simulated and observed spectra of several species for 1 .
Figure S11	The superposed simulated and observed spectra of several species in the time-dependent ESI-MS of 1
Figure S12	Graphical representation of the time dependent intensity changes of different fragments.
Figure S13	The Curie-Weiss fitting curve of susceptibility for 1 .
Figure S14	Different magnetic exchanges between nearest cobalt centres within the cluster.
Figure S15	Temperature dependence of the in-phase (χ') and out-of-phase (χ'') ac-susceptibilities at different frequencies in zero Oersted dc-field for 1 .



Scheme S1. The schematic of the synthetic procedure of **1**.

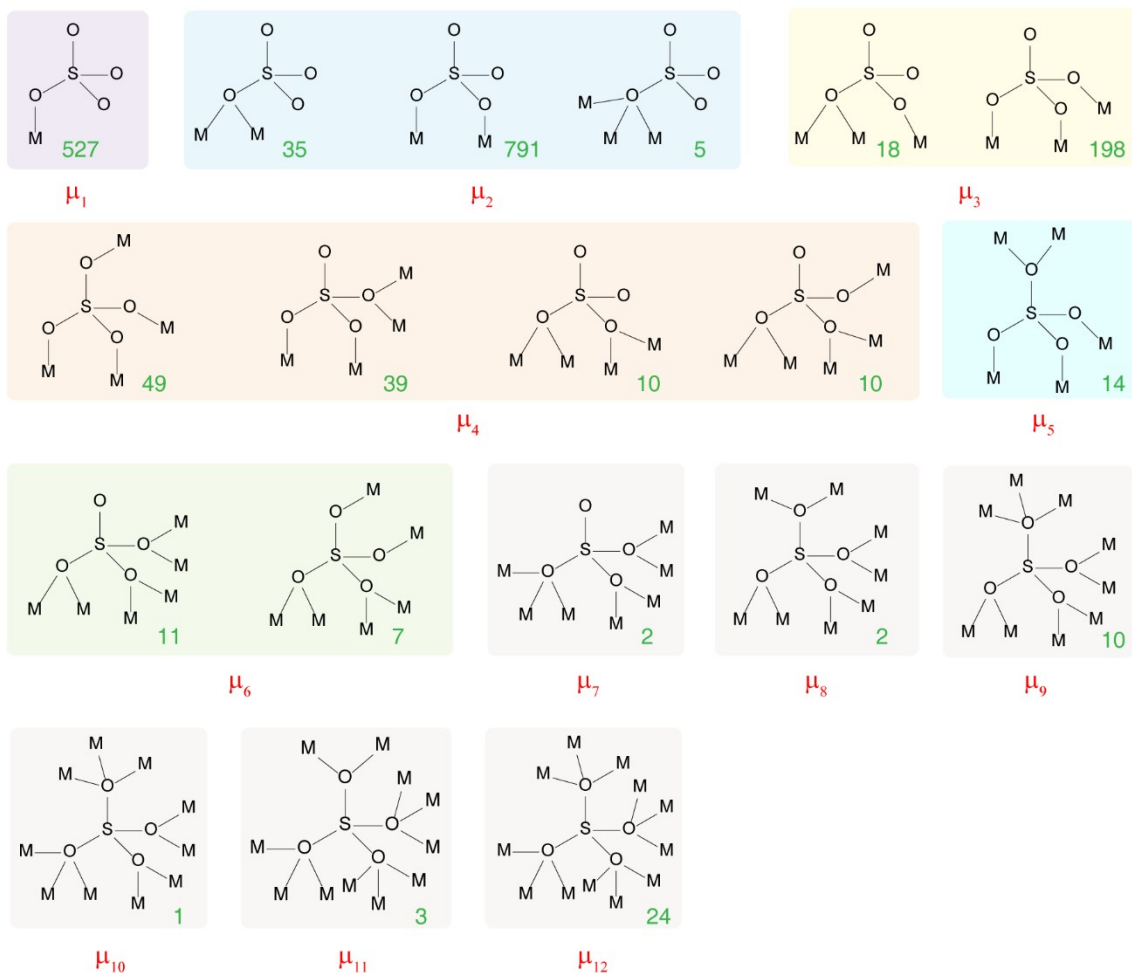
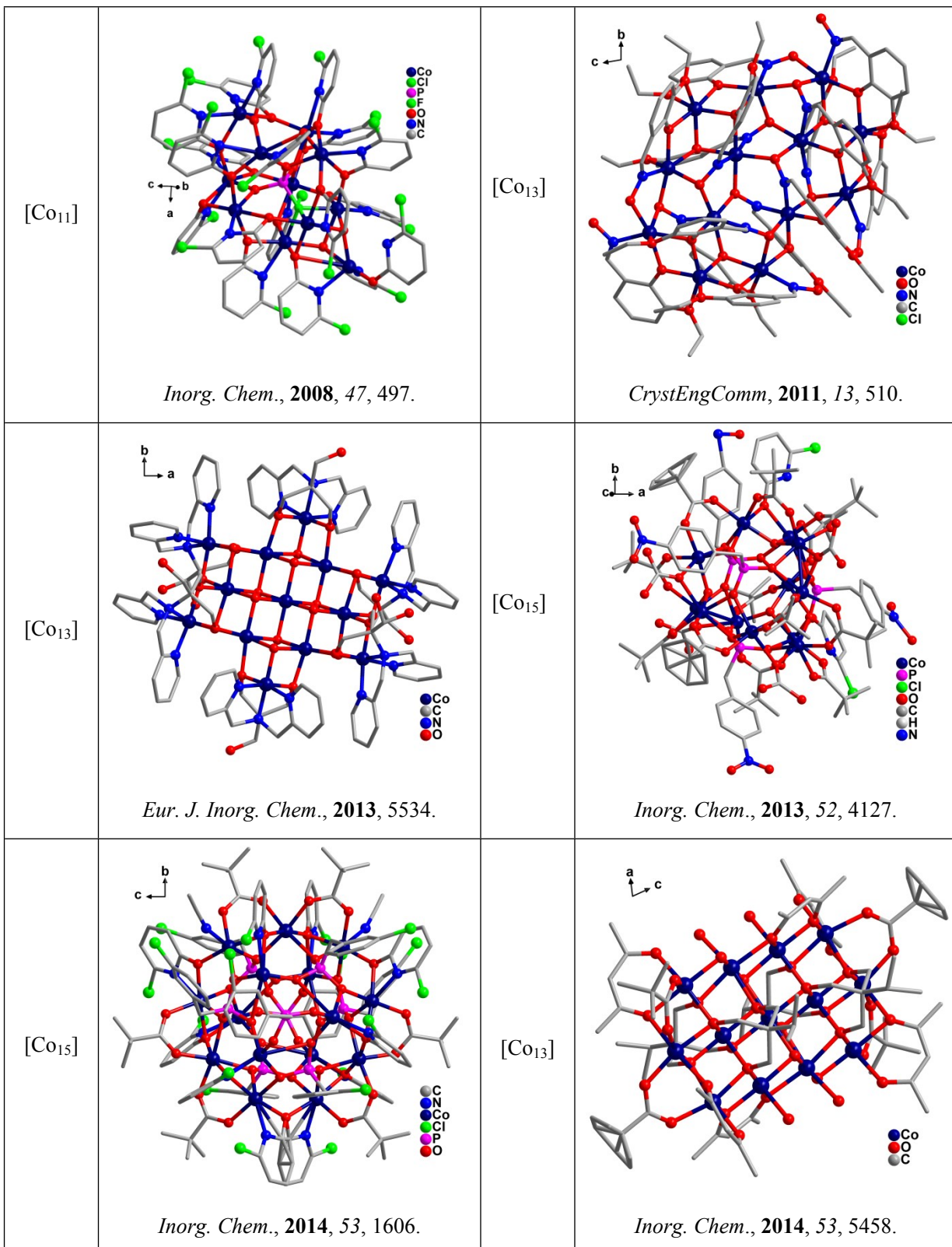


Figure S1. Statistical graph of the reported coordination models of sulphate with transition metal ions, based on the CSC data base (version 2019. 2.0.2, until 30th, Dec. 2019.). The green numbers indicates the records of each model.

Table S1. The high nuclear odd cobalt complexes (≥ 10) was searched using CSD database (Version 2019 2.0.2) until 30th, Dec. 2019.

Cluster	Structure and reference	Cluster	Structure and reference
[Co ₁₁]	 <i>Angew. Chem. Int. Ed.</i> , 1996 , <i>35</i> , 23.	[Co ₁₃]	 <i>Chem. Commun.</i> , 1996 , 1439.
[Co ₁₃]	 <i>Dalton Trans.</i> , 2000 , 3242.	[Co ₁₃]	 <i>Angew. Chem. Int. Ed.</i> , 2001 , <i>40</i> , 2700.
[Co ₁₁]	 <i>Chem. Eur. J.</i> , 2003 , <i>9</i> , 3796.	[Co ₁₉]	 <i>Angew. Chem. Int. Ed.</i> , 2008 , <i>47</i> , 9695.



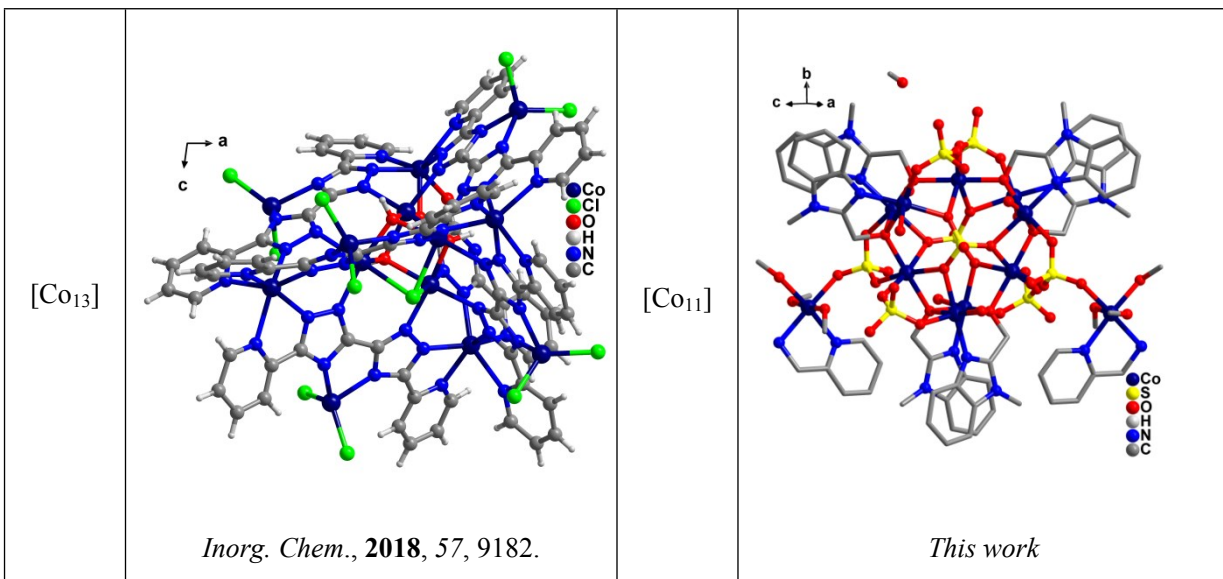


Table S2. Crystal data and refinement details for **1**.

1	
Formula	Co ₁₁ C ₇₇ H ₁₃₂ N ₁₆ S ₈ O ₅₅
Formula weight	3066.73
T (K)	100(2)
Crystal system	Monoclinic
Space group	<i>C</i> 2/ <i>c</i>
<i>a</i> (Å)	24.5656(12)
<i>b</i> (Å)	20.2178(6)
<i>c</i> (Å)	27.3542(13)
α (°)	90
β (°)	119.282(6)
γ (°)	90
<i>V</i> (Å ³)	11849.8(11)
<i>Z</i>	4
<i>D_c</i> (g cm ⁻³)	1.733
μ (mm ⁻¹)	13.91
Reflns coll.	34206
Unique reflns	10554
<i>R</i> _{int}	0.045
^a <i>R</i> ₁ [<i>I</i> ≥ 2σ(<i>I</i>)]	0.079
^b <i>wR</i> ₂ (all data)	0.243
GOF	1.07

$$^aR_1 = \sum ||F_{\text{o}}| - |F_{\text{c}}|| / \sum |F_{\text{o}}|, \quad ^b wR_2 = [\sum w(F_{\text{o}}^2 - F_{\text{c}}^2)^2 / \sum w(F_{\text{o}}^2)^2]^{1/2}$$

Table S3. Selected bond lengths (\AA) and angles ($^\circ$) of **1**.

Bond lengths					
Co1—O1	2.088 (4)	Co3—O1	2.123 (5)	Co5—O3 ⁱ	2.138 (5)
Co1—O1 ⁱ	2.088 (4)	Co3—O2	2.134 (4)	Co5—O3	2.129 (5)
Co1—O4	2.075 (5)	Co3—O5	2.077 (5)	Co5—O9	2.146 (4)
Co1—O4 ⁱ	2.075 (5)	Co3—O8	2.161 (4)	Co5—O13	2.054 (6)
Co1—O8	2.164 (5)	Co3—O20	2.079 (6)	Co5—O22	2.070 (6)
Co1—O8 ⁱ	2.164 (5)	Co3—N4	2.066 (6)	Co5—N6	2.057 (6)
Co2—O2	2.099 (4)	Co4—O1	2.105 (4)	Co6—O19	2.038 (5)
Co2—O3 ⁱ	2.100 (5)	Co4—O2	2.137 (5)	Co6—O23	2.095 (7)
Co2—O9	2.148 (4)	Co4—O10 ⁱ	2.174 (4)	Co6—O24	2.073 (7)
Co2—O10 ⁱ	2.143 (4)	Co4—O16	2.051 (5)	Co6—O25	2.131 (6)
Co2—O12	2.075 (5)	Co4—O21	2.074 (6)	Co6—N7	2.107 (9)
Co2—O17	2.092 (5)	Co4—N2	2.053 (6)	Co6—N8	2.116 (7)
Bond angles					
O1 ⁱ —Co1—O1	179.1 (2)	O1—Co3—O2	83.69 (18)	O3—Co5—O3 ⁱ	82.0 (2)
O1—Co1—O8	78.11 (17)	O1—Co3—O8	77.43 (17)	O3—Co5—O9	96.89 (18)
O1 ⁱ —Co1—O8	101.23 (17)	O2—Co3—O8	94.57 (16)	O3 ⁱ —Co5—O9	78.22 (17)
O1 ⁱ —Co1—O8 ⁱ	78.11 (17)	O5—Co3—O1	93.4 (2)	O13—Co5—O3 ⁱ	92.2 (2)
O1—Co1—O8 ⁱ	101.23 (17)	O5—Co3—O2	170.83 (18)	O13—Co5—O3	168.4 (2)
O4—Co1—O1	90.84 (18)	O5—Co3—O8	93.26 (17)	O13—Co5—O9	91.7 (2)
O4 ⁱ —Co1—O1 ⁱ	90.83 (18)	O5—Co3—O20	89.7 (2)	O13—Co5—O22	90.8 (3)
O4—Co1—O1 ⁱ	89.78 (18)	O20—Co3—O1	170.33 (19)	O13—Co5—N6	90.3 (2)
O4 ⁱ —Co1—O1	89.78 (18)	O20—Co3—O2	94.6 (2)	O22—Co5—O3	96.2 (2)
O4 ⁱ —Co1—O4	92.3 (3)	O20—Co3—O8	93.26 (19)	O22—Co5—O3 ⁱ	172.8 (2)
O4 ⁱ —Co1—O8 ⁱ	92.0 (2)	N4—Co3—O1	99.6 (2)	O22—Co5—O9	95.1 (2)
O4—Co1—O8	92.0 (2)	N4—Co3—O2	79.9 (2)	N6—Co5—O3 ⁱ	98.7 (2)
O4 ⁱ —Co1—O8	167.22 (17)	N4—Co3—O5	92.1 (2)	O19—Co6—O23	86.2 (2)
O4—Co1—O8 ⁱ	167.21 (17)	N4—Co3—O8	174.0 (2)	O19—Co6—O24	91.4 (3)
O8—Co1—O8 ⁱ	86.5 (2)	N4—Co3—O20	89.4 (2)	O19—Co6—O25	89.6 (2)
O2—Co2—O3 ⁱ	177.83 (19)	O1—Co4—O2	84.04 (18)	O19—Co6—N7	95.8 (3)
O2—Co2—O9	98.96 (16)	O1—Co4—O10 ⁱ	96.80 (16)	O19—Co6—N8	174.9 (3)

O2—Co2—O10 ⁱ	78.97 (18)	O2—Co4—O10 ⁱ	77.48 (17)	O23—Co6—O25	173.4 (3)
O3 ⁱ —Co2—O9	79.01 (18)	O16—Co4—O1	169.3 (2)	O23—Co6—N7	95.6 (3)
O3 ⁱ —Co2—O10 ⁱ	101.61 (18)	O16—Co4—O2	92.9 (2)	O23—Co6—N8	90.7 (3)
O10 ⁱ —Co2—O9	86.75 (17)	O16—Co4—O10 ⁱ	92.5 (2)	O24—Co6—O23	90.6 (3)
O12—Co2—O2	90.22 (19)	O16—Co4—O21	88.9 (2)	O24—Co6—O25	84.4 (3)
O12—Co2—O3 ⁱ	89.18 (19)	O16—Co4—N2	90.3 (2)	O24—Co6—N7	170.8 (4)
O12—Co2—O9	94.7 (2)	O21—Co4—O1	96.3 (2)	O24—Co6—N8	92.6 (3)
O12—Co2—O10 ⁱ	169.18 (19)	O21—Co4—O2	167.2 (2)	N7—Co6—O25	89.9 (3)
O12—Co2—O17	88.6 (2)	O21—Co4—O10 ⁱ	89.8 (2)	N7—Co6—N8	80.5 (4)
O17—Co2—O2	91.47 (18)	N2—Co4—O1	80.2 (2)	N8—Co6—O25	93.9 (3)
O17—Co2—O3 ⁱ	90.6 (2)	N2—Co4—O2	99.7 (2)	Co2 ⁱ —O3—Co5 ⁱ	98.33 (19)
O17—Co2—O9	169.04 (19)	N2—Co4—O10 ⁱ	176.1 (2)	Co2 ⁱ —O3—Co5	117.9 (2)
O17—Co2—O10 ⁱ	91.98 (18)	N2—Co4—O21	93.0 (3)	Co5—O3—Co5 ⁱ	98.0 (2)
Co1—O1—Co3	99.79 (18)	Co2—O2—Co3	121.36 (19)	Co3—O8—Co1	96.26 (16)
Co1—O1—Co4	119.2 (2)	Co2—O2—Co4	98.9 (2)	Co5—O9—Co2	96.62 (17)
Co4—O1—Co3	96.71 (18)	Co3—O2—Co4	95.43 (17)	Co2 ⁱ —O10—Co4 ⁱ	96.41 (18)
Symmetry code: (i) -x+1, y, -z+1/2.					

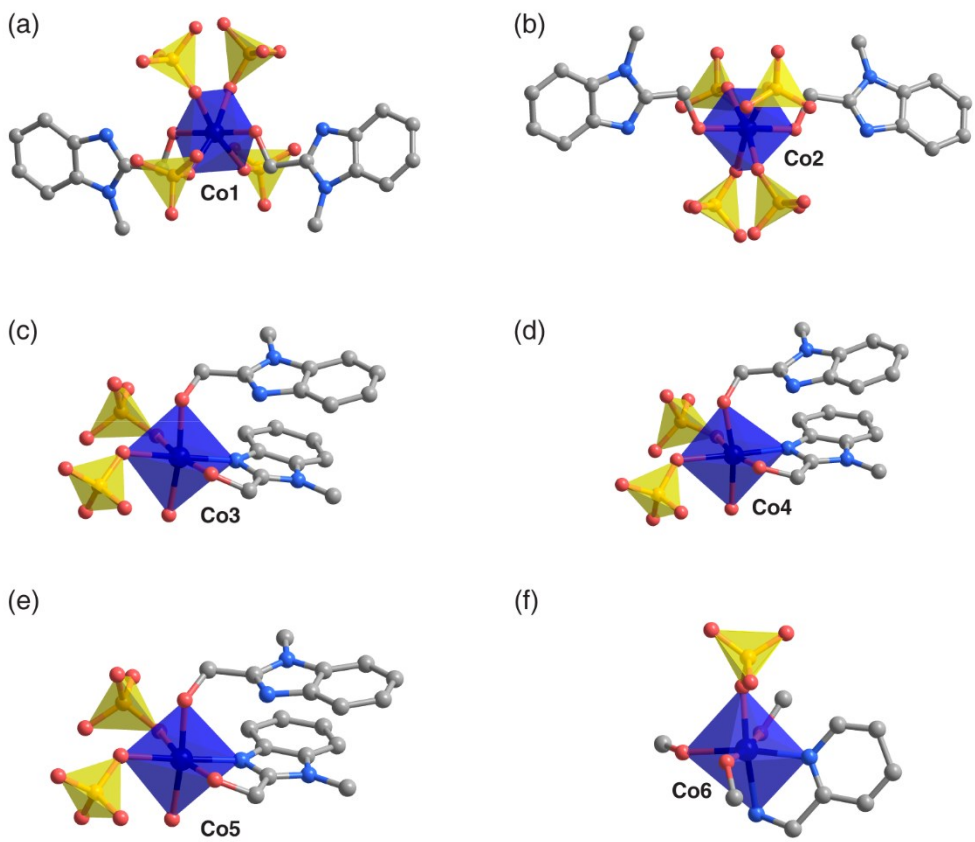


Figure S2. View of the coordination geometry of different cobalt ions in **1**.

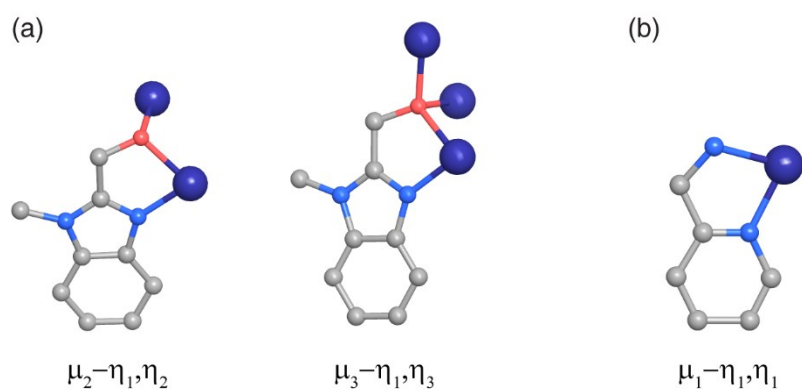


Figure S3. View of the coordination model of the *mbm* and *pma* ligands.

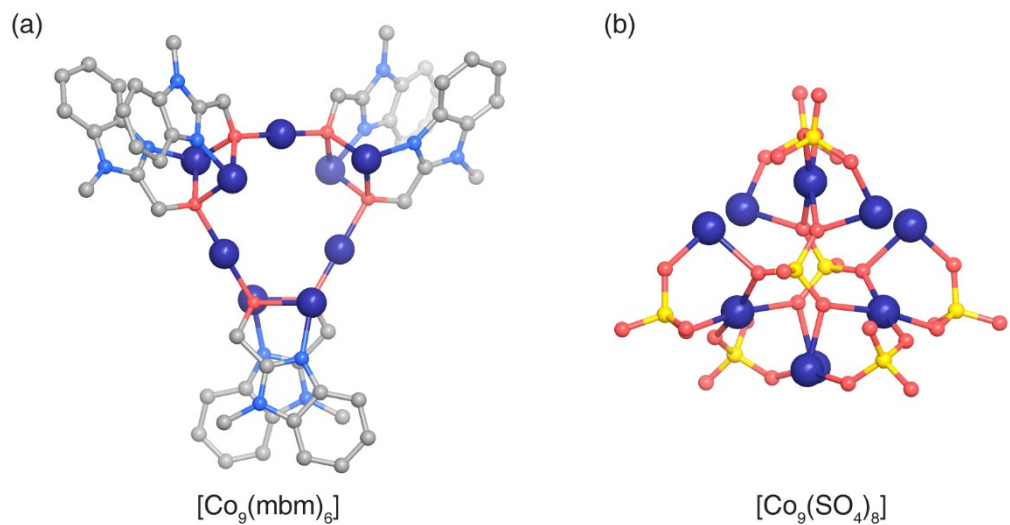


Figure S4. View of linkage of the [Co₉] inner core through *mbm*⁻ (a) and SO₄²⁻ (b), respectively.

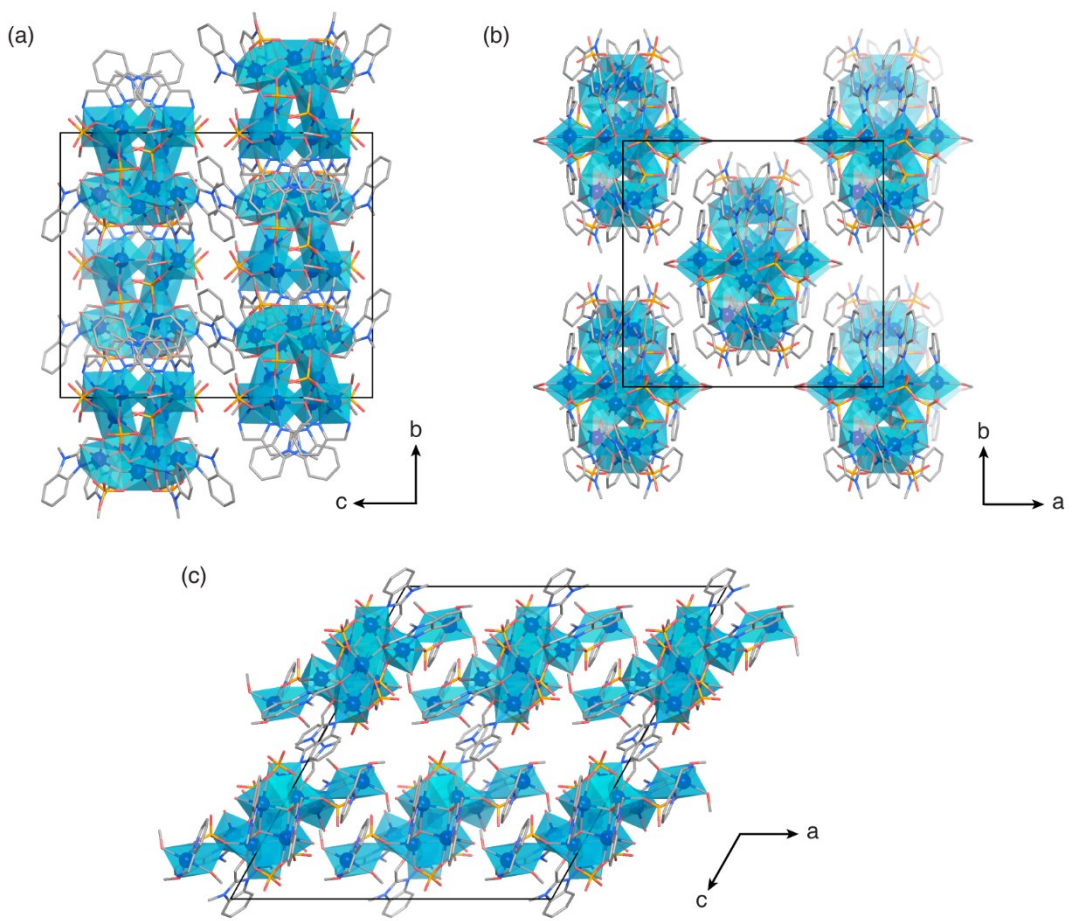


Figure S5. View of the packing model of **1** along crystallographic *a* (a), *c* (b) and *b* (c) directions. $[Co_9]$ inner core through mbm^- (a) and SO_4^{2-} (b), respectively.

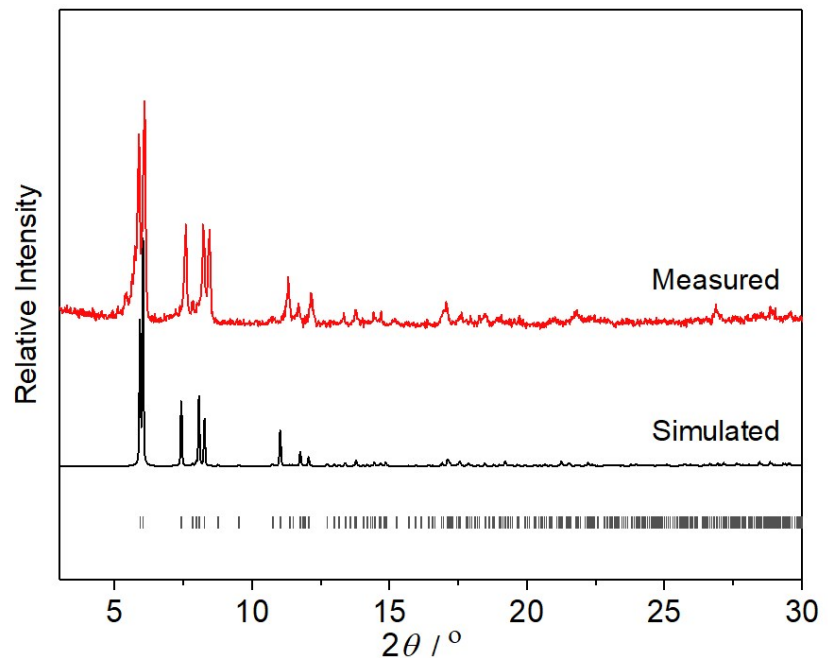


Figure S6. The measured and simulated PXRD data for **1**.

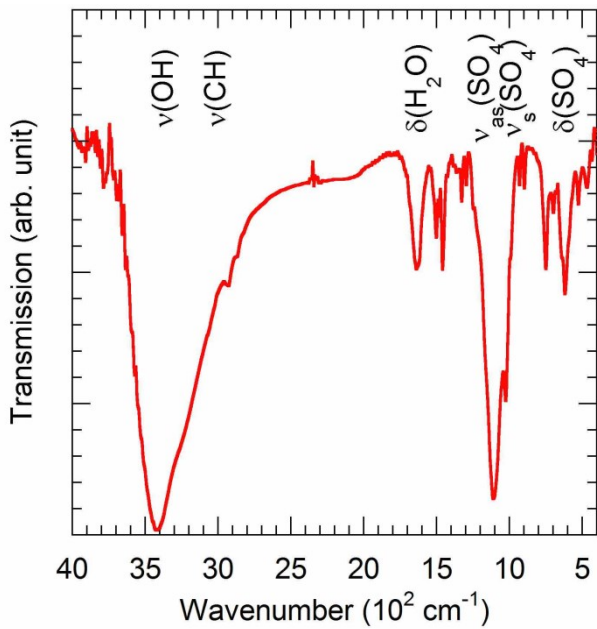


Figure S7. Infrared transmission spectrum of **1**. The mid-infrared spectrum of **1** is dominated by the sulfate and water vibrations. Those of the ligands are obscured by them. The broad and strong collection of bands belonging to both symmetric and antisymmetric stretching modes of the coordinated and solvent water molecules as well as those of the methanol does not allow for any specific assignment. The bending of the water exhibits a medium strength band centered at 1619 cm^{-1} . The other very strong band represent the antisymmetric mode of the three crystallographically different sulfate ions with possibly a sharp shoulder peak ca. 980 cm^{-1} from the symmetric vibration. The bending mode of the sulfate shows a structured broad band at ca. 650 cm^{-1} . The vibration of the organic ligands are rather weak in comparison.

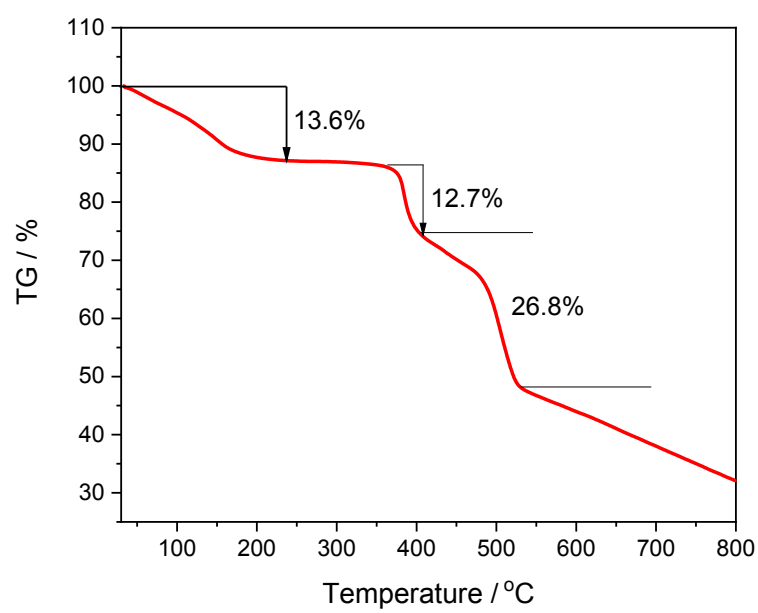


Figure S8. Thermogravimetry for **1** under nitrogen atmosphere showing the sequential loss of solvents and ligands to form a purely Co-SO₄ solid.

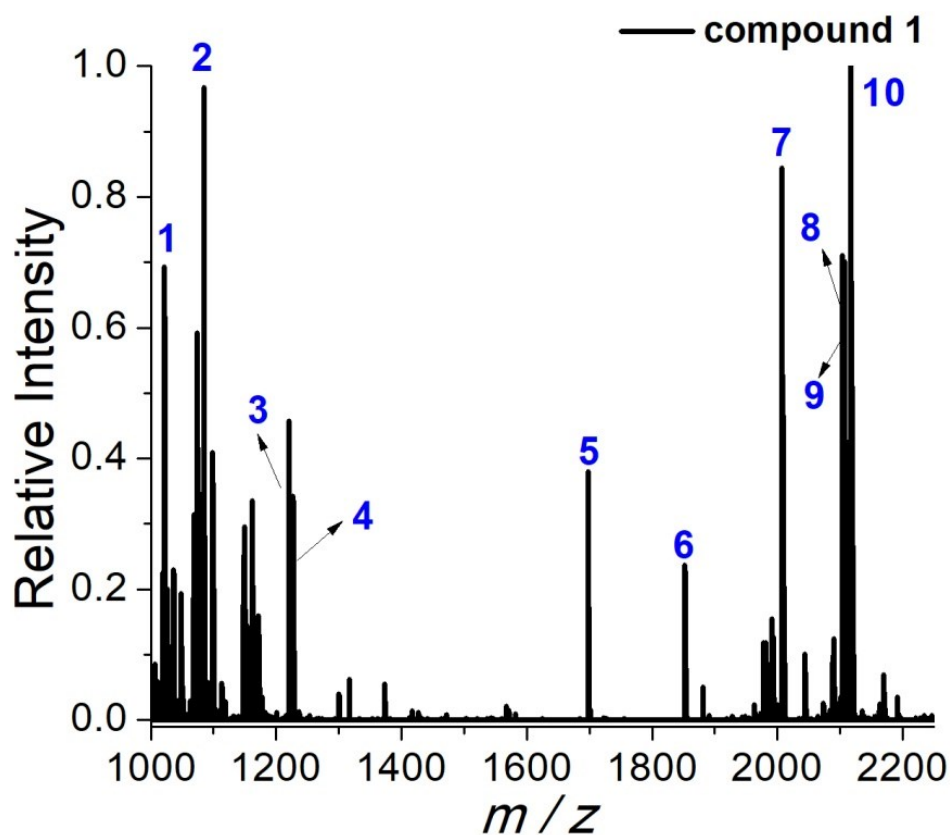


Figure S9. Negative ESI-MS spectra of **1** in CH₃OH (In-Source CID 0 eV).

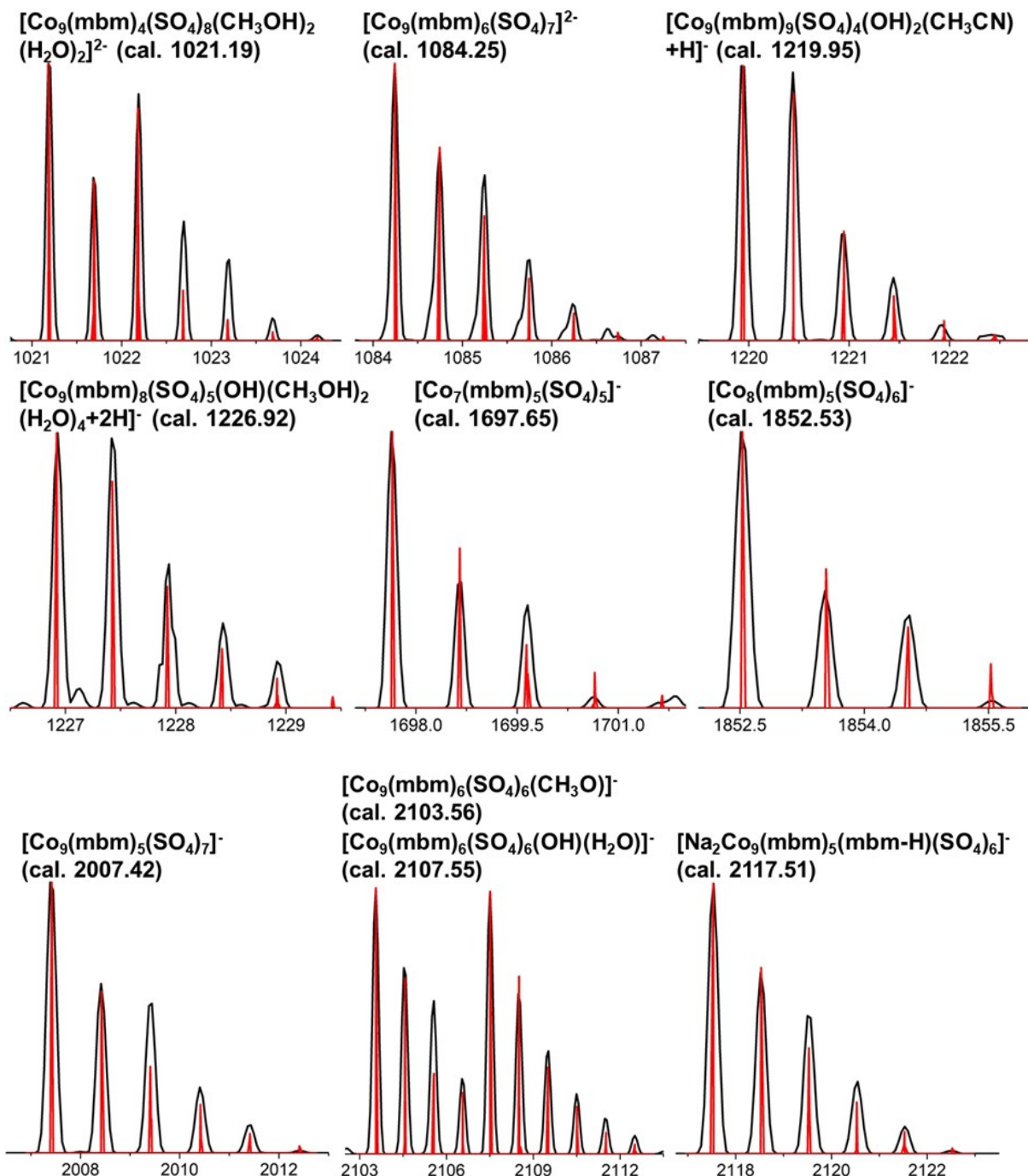


Figure S10. The superposed simulated and observed spectra of several species for **1** (In-Source CID 0 eV).

Table S4. Major species assigned in the ESI-MS of **1** in negative mode.

Peaks	1 (In-Source CID 0 eV)			
	Formular	Relative Intensity	Obs. m/z	Calc. m/z
1	[Co ₉ (mbm) ₄ (SO ₄) ₈ (CH ₃ OH) ₂ (H ₂ O) ₂] ²⁻	0.693	1021.18	1021.19
2	[Co ₉ (mbm) ₆ (SO ₄) ₇] ²⁻	0.968	1084.24	1084.25
3	[Co ₉ (mbm) ₉ (SO ₄) ₄ (OH) ₂ (CH ₃ CN)+H] ⁻	0.458	1219.93	1219.95
4	[Co ₉ (mbm) ₈ (SO ₄) ₅ (OH)(CH ₃ OH) ₂ (H ₂ O) ₄ +HH] ⁻	0.342	1226.93	1226.92
5	[Co ₇ (mbm) ₅ (SO ₄) ₅] ⁻	0.381	1697.64	1697.65
6	[Co ₈ (mbm) ₅ (SO ₄) ₆] ⁻	0.237	1852.51	1852.53
7	[Co ₉ (mbm) ₅ (SO ₄) ₇] ⁻	0.844	2007.39	2007.42
8	[Co ₉ (mbm) ₆ (SO ₄) ₆ (CH ₃ O)] ⁻	0.711	2103.56	2103.56
9	[Co ₉ (mbm) ₆ (SO ₄) ₆ (OH)(H ₂ O)] ⁻	0.701	2107.51	2107.55
10	[Co ₉ (mbm) ₅ (mbm-H)(SO ₄) ₆ Na ₂] ⁻	1	2117.54	2117.51

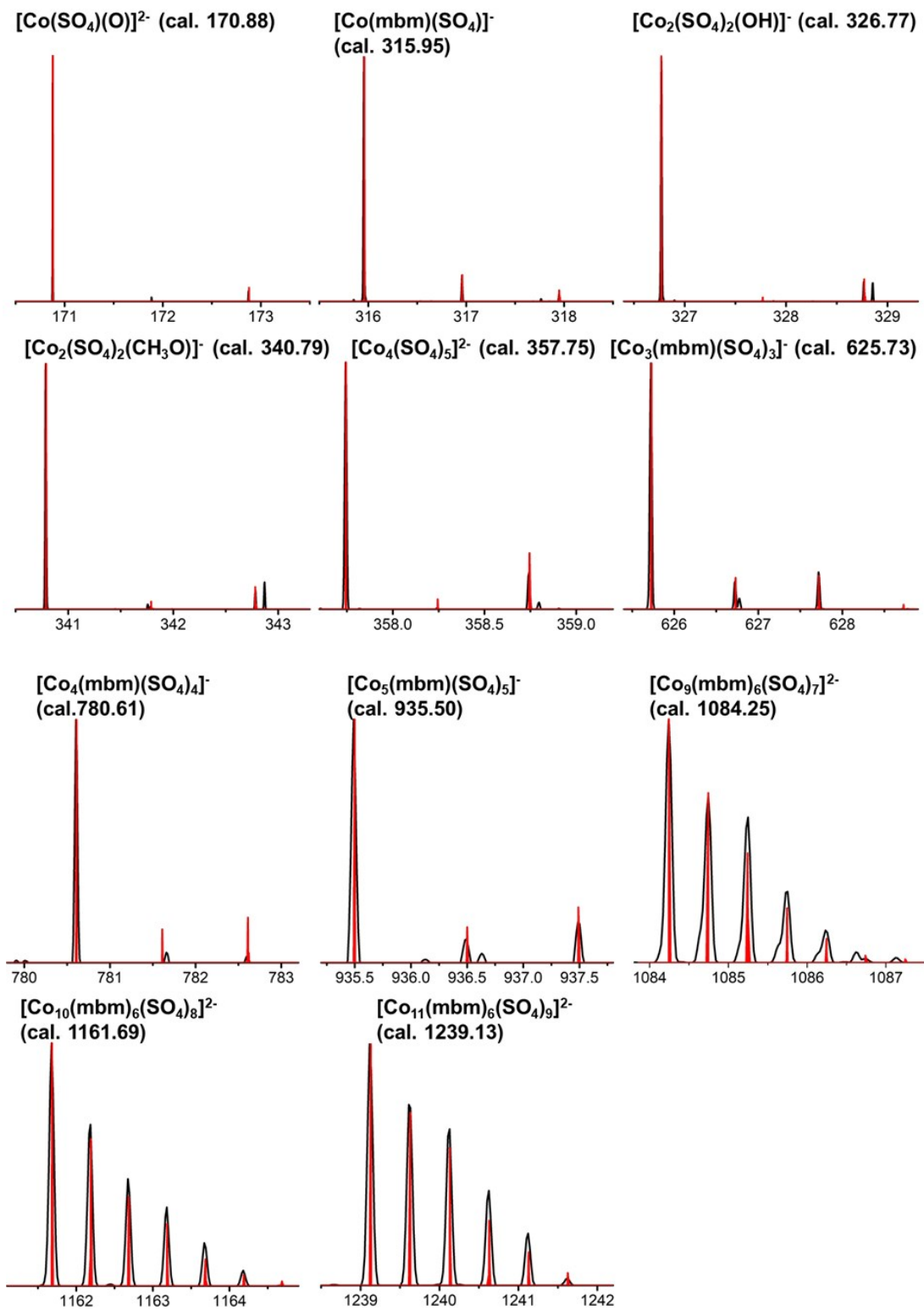


Figure S11. The simulated and observed spectra of several species in the time-dependent ESI-MS of **1** in negative mode.

Table S5. Time-dependent ESI-MS spectra assigned in the ESI-MS of **1** in negative mode. The highest intensity is highlighted in red.

Fragment	Relative Intensity at different time								
	0min	5min	10 min	20 min	30 min	1 h	2 h	4 h	12 h
[Co(SO ₄)(O)] ²⁻ (cal. 170.88)	1	1	1	1	1	1	1	1	0.713
[Co(mbm)(SO ₄)] ⁻ (cal. 315.95)	0.041	0.158	0.229	0.281	0.138	0.199	0.154	0.137	0.112
[Co ₂ (SO ₄) ₂ (OH)] ⁻ (cal. 326.77)	0.182	0.572	0.776	0.952	0.839	0.807	0.696	0.570	0.071
[Co ₂ (SO ₄) ₂ (CH ₃ O)] ⁻ (cal. 340.79)	0.171	0.542	0.750	0.970	0.831	0.788	0.710	0.549	0.068
[Co ₄ (SO ₄) ₅] ²⁻ (cal. 357.75)	0.065	0.202	0.279	0.306	0.310	0.263	0.267	0.222	0.013
[Co ₃ (mbm)(SO ₄) ₃] ⁻ (cal. 625.73)	0.058	0.152	0.219	0.255	0.489	0.853	0.700	0.419	0.048
[Co ₄ (mbm)(SO ₄) ₄] ⁻ (cal. 780.61)	0.011	0.029	0.042	0.054	0.113	0.182	0.216	0.130	0.005
[Co ₅ (mbm)(SO ₄) ₅] ⁻ (cal. 935.50)	0	0.005	0.008	0.011	0.048	0.103	0.118	0.152	0.289
[Co ₉ (mbm) ₆ (SO ₄) ₇] ²⁻ (cal. 1084.25)	0	0	0	0.015	0.019	0.275	0.430	0.526	1
[Co ₁₀ (mbm) ₆ (SO ₄) ₈] ²⁻ (cal. 1161.69)	0	0	0	0.014	0.064	0.266	0.402	0.475	0.903
[Co ₁₁ (mbm) ₆ (SO ₄) ₉] ²⁻ (cal. 1239.13)	0	0	0	0.007	0.035	0.123	0.215	0.243	0.462

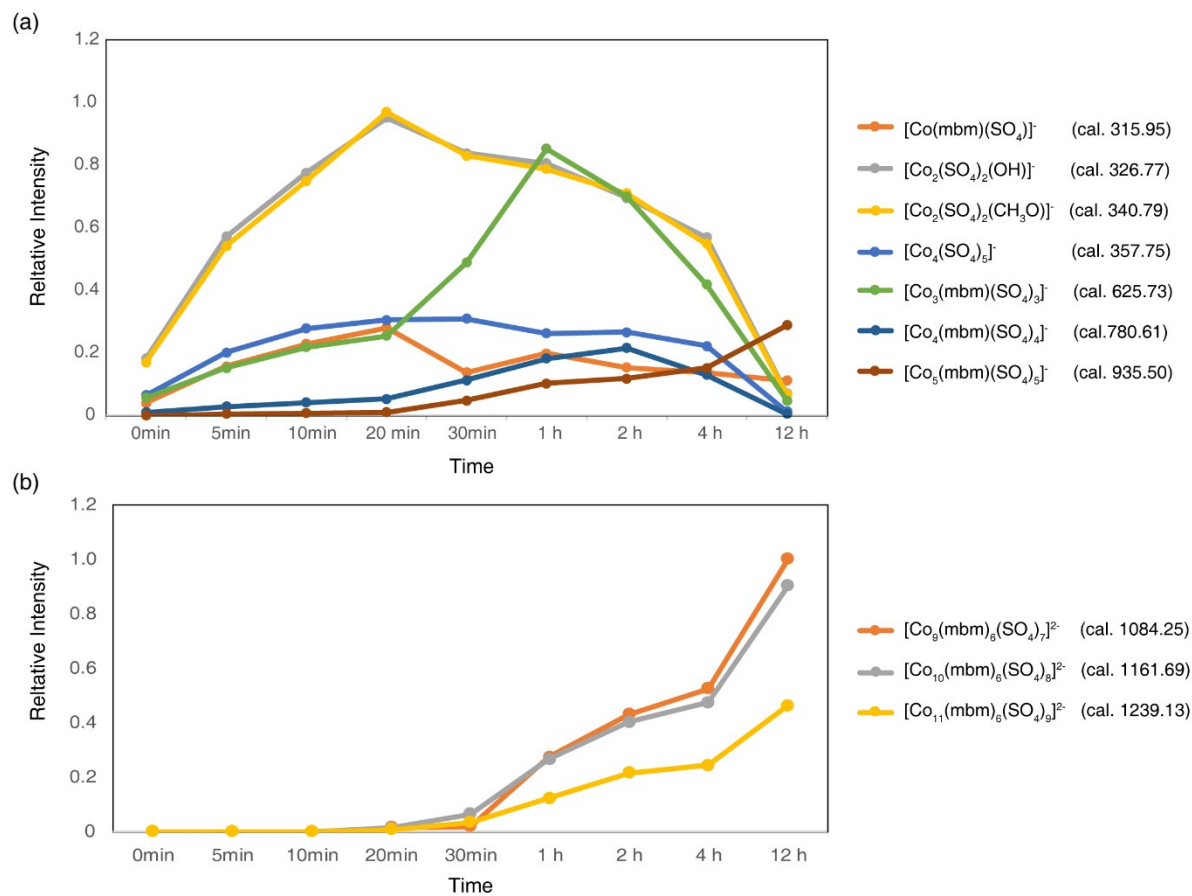


Figure S12. Graphical representation of the time dependent intensity changes of different fragments.

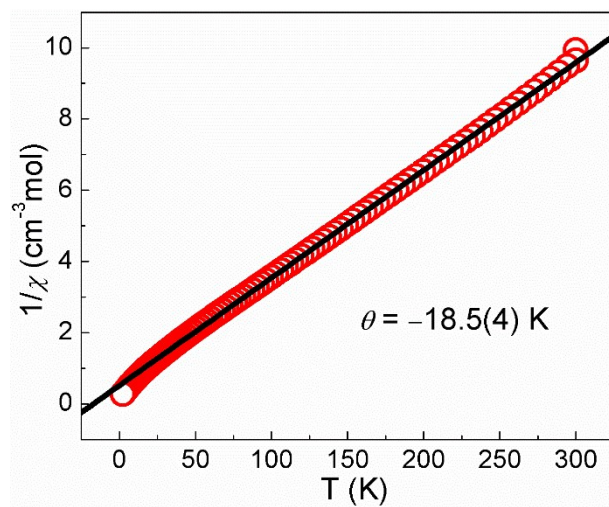


Figure S13. The Curie-Weiss fitting curve of susceptibility for **1** over the temperature range of 100~290 K.

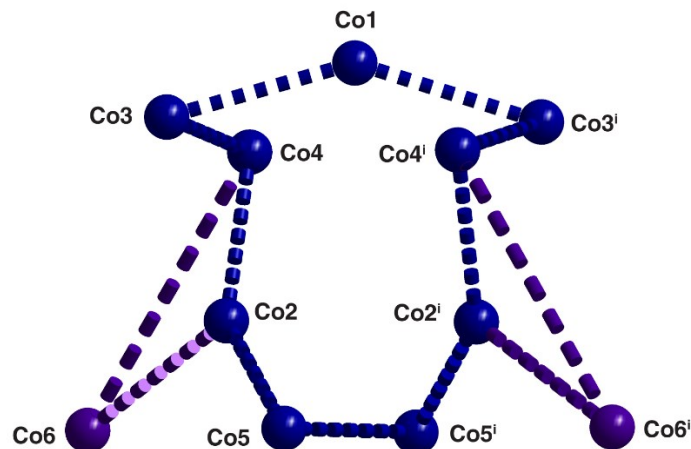


Figure S14. Different magnetic exchanges between nearest cobalt centres within the cluster. Symmetry code: (i) $-x+1, y, -z+1/2$.

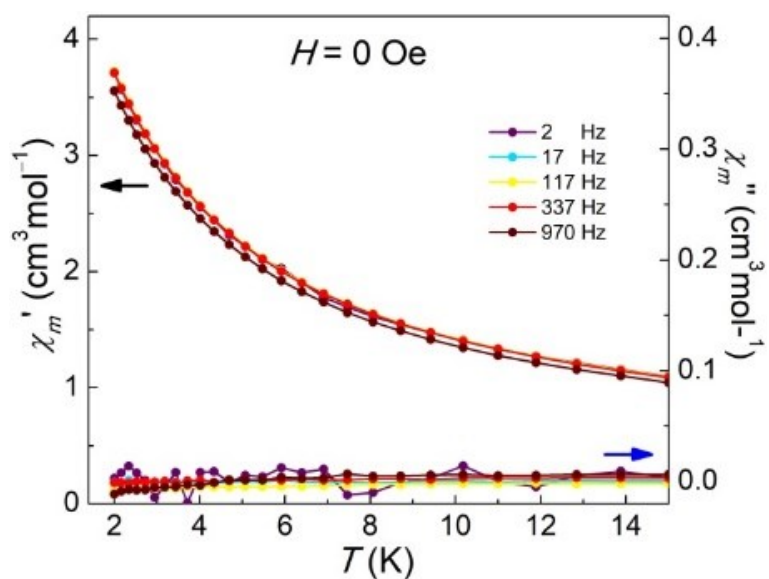


Figure S15. Temperature dependence of the in-phase (χ') and out-of-phase (χ'') ac-susceptibilities at different frequencies in zero Oersted dc-field for **1**.